Chinese Journal of
POLYMER SCIENCE

RESEARCH ARTICLE

https://doi.org/10.1007/s10118-024-3120-x
Chinese J. Polym. Sci.

Unconventional Fluorescent and Multi-responsive Polyethyleneimine with LCST and UCST Behavior: Synthesis, Characterization and Biological Applications

Feng-Ming Yin[a], Li-Li Wu[b], Shu-Sheng Li[a,c*], Xiao-Na Pan[a], Xiao-Li Zhu[a*], Xu-Bao Jiang[a], and Xiang Zheng Kong[a]

[a] *College of Chemistry and Chemical Engineering, University of Jinan, Jinan 250022, China*
[b] *Shandong Institute for Product Quality Inspection, Jinan 250102, China*
[c] *College of Chemical Engineering, Tianjin University, Tianjin 300072, China*

Electronic Supplementary Information

Abstract Non-aromatic fluorescent and multi-responsive materials, exhibiting inherent fluorescence emission and controlled phase change, have garnered significant attention in recent years. However, the underlying interaction between their fluorescent properties and phase transition remains unclear. In this study, we synthesized a series of catalyst-free aza-Michael addition-based polyethyleneimine (RFPEI) materials by reacting polyethyleneimine (PEI) with *N*-isopropyl acrylamide (NIPAM). The resulting RFPEI was comprehensively characterized, and demonstrated dual-phase transition behavior (LCST and UCST) in water, which could be finely tuned by adjusting its composition or external factors such as pH. Notably, upon UV irradiation (365 nm), RFPEI exhibited strong fluorescence emission. We further investigated the effects of NIPAM grafting percentage to PEI, polymer concentration, and pH on the LCST/UCST and fluorescent properties of RFPEI aqueous solutions. Moreover, we showcased the great potential of RFPEI as a versatile tool for physiological cell imaging, trace detection, and controlled release of doxorubicin. Our study presents a novel class of stimuli-responsive fluorescent materials with promising applications in the field of biomedicine.

Keywords Polyethyleneimine; Multi-responsiveness; Intrinsic fluorescence emission; Cell imaging; Controlled drug release

Citation: Yin, F. M.; Wu, L. L.; Li, S. S.; Pan, X. N.; Zhu, X. L.; Jiang, X. B.; Kong, X. Z. Unconventional fluorescent and multi-responsive polyethyleneimine with LCST and UCST behavior: synthesis, characterization and biological applications. *Chinese J. Polym. Sci*. https://doi.org/10.1007/s10118-024-3120-x

INTRODUCTION

Multi-stimulus responsive fluorescent polymers (SRFPs) exhibit significant changes in their physical and chemical properties, particularly fluorescent properties, when subjected to slight variations in the external environment. This unique characteristic has led to the widespread utilization of SRFPs in various fields, including controlled drug release,[1–3] cell imaging,[4] intelligent detection,[5,6] and display materials.[7]

Traditionally, SRFPs are prepared by physically or chemically coating or bonding fluorogens, such as transition metal ions,[2,6] quantum dots,[3,8] and conjugated fluorescent dyes,[4,5] onto the stimuli-responsive polymer. However, these fluorogens have several noticeable drawbacks. Metal ions and quantum dots suffer from poor chemical stability and high cytotoxicity, while conjugated organic dyes tend to leak and possess low water solubility. Furthermore, they often exhibit aggregation-caused quenching (ACQ) effects at high concentrations, limiting their applications in real-time biological detection, medicine, and other fields. To overcome these limitations, a series of SRFPs were designed and synthesized by combining aggregation-induced emission fluorogens (AIEgens) with stimuli-responsive polymers.[1,9–12] The concept of AIE was introduced by Tang *et al.*,[13–15] offering a solution to the challenges associated with ACQ.

The properties of cluster-triggered emission (CTE) polymers that contain heteroatomic groups, such as amine, carbonyl, and ether, differentiate them from aromatic AIEgens. These CTE polymers are well-known for their hydrophilicity, non-toxicity, and biocompatibility, which makes them a promising area of research within the field of fluorescent polymers.[16–22] In our previous studies, we focused on understanding the emission mechanism of various CTE polymers. Specifically, we investigated polyurea,[23] poly(ethylene glycol),[24–26] polyamide and amide salt[27,28] and silicon-containing polymers.[29,30] Through systematic analysis, we determined the influence of molecular structure, the forms in which these polymers exist, and environmental factors on their fluorescence emissions. Moreover, we explored the advantages offered by these CTE polymers for a range of applications. For instance, we employed them in cell imaging,[25,28]

* Corresponding authors, E-mail: chm_liss@ujn.edu.cn (S.S.L.)
E-mail: chm_zhuxl@ujn.edu.cn (S.S.L.)

Received January 31, 2024; Accepted March 6, 2024; Published online April 15, 2024

detection of metal ions,[23,25,27,29] and identification of drugs.[24,26] Leveraging the unique properties of these polymers allows us to develop innovative solutions in various fields.

Stimuli-responsive polymers exhibit changes in their molecular conformation in response to variations in temperature, resulting in alterations in their hydrophilicity and solubility. Depending on their phase transition behavior, these polymers can be categorized as high critical solution temperature (UCST) type,[31] low critical solution temperature (LCST) type,[32] or a combination of both.[33,34] While the transformation behavior between LCST and UCST can be achieved by modifying the solvent or polymer composition,[33,35] the research on polymers that exhibit both LCST and UCST in pure water holds greater practical value. Understanding the conformational changes in CTE polymers induced by environmental stimuli is crucial as it directly affects their cluster state and fluorescence emission. Investigating the correlation between these two changes can provide insights into the mechanism underlying CTE. However, there is limited research exploring the relationship between fluorescence emission and the phase transition behavior of CTE polymers responsive to environmental stimuli.[30,36]

The objective of this study was to synthesize a multi-stimulus responsive cluster-induced fluorescent polyethyleneimine (RFPEI) using a catalyst-free aza-Michael addition reaction. The reaction involved combining *N*-isopropyl acrylamide (NIPAM) and the ethylene imine unit (-CH_2-CH_2-NH-, EI) in polyethyleneimine (PEI). RFPEI exhibited both LCST and UCST responses, meaning that it underwent phase transitions with changes in temperature. Additionally, RFPEI demonstrated pH responsiveness in aqueous solutions. It also displayed robust CTE in response to temperature and pH variations. The relationship between phase transition behavior and fluorescence emission was investigated in this study. Factors such as the percentage of NIPAM grafting on PEI, polymer concentration, and pH level of aqueous solutions were evaluated for their impact on the phase transition behavior and fluorescent properties of RFPEI. Furthermore, the utility of RFPEI was demonstrated in various applications. It was used for cell imaging and showed promise in trace detection and controlled release of doxorubicin (DOX), a widely used anticancer drug. Overall, this research presents the synthesis and characterization of RFPEI, showcasing its multi-stimuli responsiveness and potential applications in biomedicine.

EXPERIMENTAL

Materials

Polyethyleneimine (PEI, AR, M_n=1800), *N*-isopropyl acrylamide (NIPAM, AR), and adriamycin hydrochloride (DOX, 98%) were purchased from Aladdin Chemical (Shanghai, China). Ethanol, sodium hydroxide (NaOH, AR) and hydrochloric acid (HCl, AR) were purchased from Tianjin Fuyu Fine Chemical Co., Ltd., (Tianjin, China). The deionized water with a resistivity of 18.2 MΩ·cm was prepared in the laboratory.

Synthesis of RFPEI

The synthesis of RFPEI involved a catalyst-free aza-Michael addition reaction using NIPAM and PEI at specific molar ratios. In a typical reaction, 1.81 g (16 mmol) of NIPAM and 0.86 g (20 mmol of EI unit) of PEI were dissolved in 20 mL of ethanol. The mixture was stirred at room temperature until the disappearance of the double bond peak of NIPAM, which was confirmed by ^{1}H-NMR analysis conducted at regular intervals of 0.5 h. After the completion of the reaction, the ethanol solvent was removed using rotary evaporation, resulting in the formation of a viscous RFPEI product. A series of RFPEI samples were prepared by adjusting the molar ratio of NIPAM/EI according to Table 1, following the same procedure described above.

Table 1 Synthesis of RFPEI with varied NIPAM/EI molar ratios and the corresponding data of GPC.

Sample	NIPAM/EI (mol)		GPC [a]	
	Feeding	By ^{1}H-NMR	M_n	PDI
P0	0/5	–	–	–
P1	1/5	0.95/5	2200	1.07
P2	2/5	1.8/5	2400	1.11
P3	3/5	2.7/5	3100	1.10
P4	4/5	3.8/5	3700	1.37
P5	5/5	4.2/5	4000	1.53

[a] GPC data examined in DMF at 1.0 mg/mL

Characterizations

Chemical structure of RFPEI was detected by Nuclear Magnetic Resonance (NMR, Advance III, Brüker, USA, 400 MHz) using D_2O as solvent, and by Fourier transform infrared spectroscopy (FTIR, Tensor 27, Brüker, USA) by KBr tablet at the range of 4000–400 cm^{-1}. Molecular weight of RFPEI was measured by gel permeation chromatography (GPC, Viscotek TDA305max, Malvern, Britain) at 25 °C using DMF as solvent. Particle size and size distribution of RFPEI in water and mixed solution were measured by dynamic light scattering (DLS, Nano-ZS, Malvern, Britain). The transmittance of RFPEI in water (1.0–100.0 mg/mL) was measured by UV spectrophotometer at 600 nm (UV, Lambda 35, PerkinElmer, USA) equipped with a HAAKE temperature controller, and the temperature raised from 20 °C to 80 °C at a rate of 2 °C/min. Moreover, the temperature at which the transmittance reaches to 50% is defined as LCST or UCST value. The pH of RFPEI aqueous solution was recorded by a potential titrator (808 Titrando, Metrohm, Switzerland), and the pH was adjusted to desired value using 0.2 mol/L NaOH or HCl solution. The fluorescent properties of RFPEI aqueous solution were tested using a fluorescence spectrometer (F-7000, Hitachi, Japan) with an excitation and emission slit width of 2.5 nm and a voltage of 700 V.

RESULTS AND DISCUSSION

Synthesis and Characterization of RFPEI

The synthesis of RFPEI involved the aza-Michael addition reaction between NIPAM and PEI at different molar ratios. During this reaction, the electron-deficient double bond of NIPAM, which is attached to an electron-withdrawing carbonyl group, was attacked by the adipic amine and imine groups of PEI. Adipic amine and imine groups possess strong alkalinity and lone pair electrons, making them suitable nucleophiles for the reaction. The aza-Michael addition reaction occurred spontaneously at room temperature without the need for any catalyst.[30,32,37–39] This demonstrates the facile and versatile na-

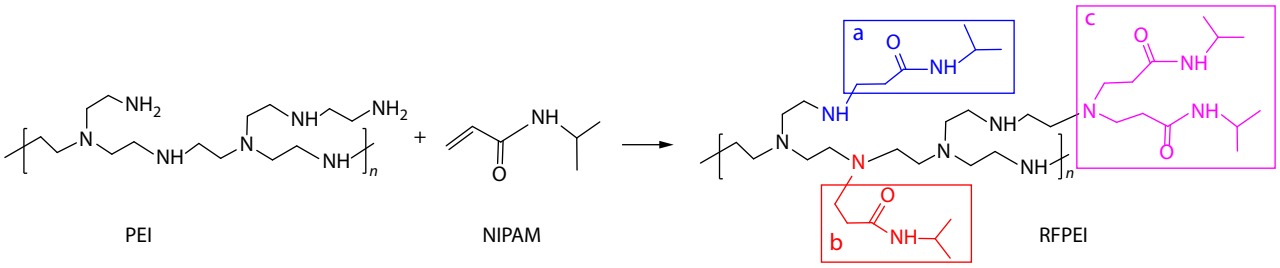

Scheme 1 Synthesis of RFPEI through aza-Michael addition of NIPAM to PEI.

ture of the synthesis method, which relies on the distinctive chemical properties of the reactants involved: the electron deficiency of NIPAM and the strong alkalinity of PEI's amine and imine groups. The addition reaction between NIPAM and PEI can be categorized into three distinct forms, as illustrated in Scheme 1. In the first form (blue region a), a single addition reaction takes place between NIPAM and the amine group located on the side chain of PEI. In the second form (red region b), NIPAM is added to the imine group located on the main chain of PEI. Finally, in the third form (purple region c), NIPAM undergoes a secondary addition reaction with the imine group formed after the primary addition.

In summary, the addition reaction between NIPAM and PEI can occur in three different forms, each with varying activity levels and reaction sequences. The aza-Michael addition mechanism explains that the imine group on the main chain of PEI is more basic than the amine group on the branch chain, resulting in higher addition activity. However, the steric hindrance of the amine group on the branch chain is smaller than that of the imine group on the main chain, increasing the probability of reaction. When the amount of NIPAM is limited, the primary addition reactions predominantly occur in the blue zone (a) and the red zone (b). As the amount of NIPAM increases, it tends to undergo secondary addition with the imine group formed through the primary addition, once the basic reaction between the amine group on the branch chain and the imine group on the main chain is complete. Regardless of the number of branches in PEI, the molar amount of active hydrogen in the amine and imine groups is equivalent to the molar amount of EI. This suggests that by adjusting the molar ratio of NIPAM/EI, it is possible to link different levels of NIPAM to the PEI molecular chain. This is further demonstrated in Table 1.

The chemical structures of PEI, NIPAM and RFPEI (P4) were characterized using ^{1}H-NMR and ^{13}C-NMR spectroscopy, as shown in Fig. 1 and Table S1 and S2 (in the electronic supplementary information, ESI). In the ^{1}H-NMR spectrum of PEI (Fig. 1a), the methylene group shows a consistent chemical environment, resulting in a single peak at 2.5 ppm (H1, H2).[40] The ^{1}H-NMR spectrum of NIPAM (Fig. 1b) displays four characteristic peaks for the H proton. H4, located within the double bond, appears as two separate peaks at 5.6 and 6.0 ppm due to *cis-trans* isomerism. The methylene group (H8) exhibits a peak at 3.8 ppm, which can be attributed to the electron-withdrawing effect of the amide group. Additionally, the methyl group (H9) shows a characteristic peak at 1.0 ppm.[32] In the P4 spectrum (Fig. 1c), the chemical shifts of the methylene (H1, H2) in PEI, as well as the isopropyl (H8, H9) in NIPAM remain relatively unchanged compared to their respective individual spectra. Notably, the characteristic peaks of the double bond (H4, H5) in NIPAM almost completely disappear in the P4 spectrum. Instead, two new peaks appear at 2.1 ppm and 2.7 ppm. These peaks correspond to the methylene groups (H4 and H5) formed after aza-Michael addition, con-

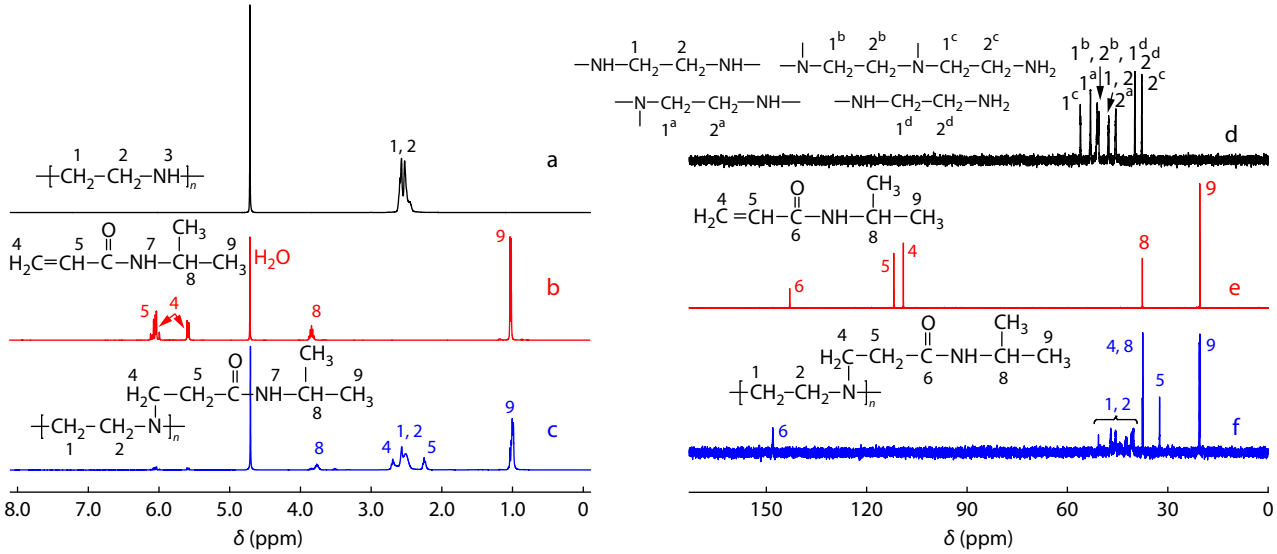

Fig. 1 (a–c) ^{1}H-NMR and (d–f) ^{13}C-NMR spectra of (a, d) PEI, (b, e) NIPAM and (c, f) P4.

https://doi.org/10.1007/s10118-024-3120-x

nected with the imine and carbonyl groups, respectively.[32,41] However, it is important to note that the amine/imine protons readily undergo substitution with deuterium from D_2O. Consequently, no distinct characteristic peak of the amine/imine groups is observed in the spectrum. Instead, a peak attributable to H_2O formed after proton substitution is detected at 4.7 ppm.

The ^{1}H-NMR spectra of all the RFPEI samples (P1–P5) were shown in Fig. S1 (in ESI), and the resulting data matched the analysis results mentioned above. By comparing the integral area of characteristic peaks for methylene (H1, H2) in PEI and methyl (H9) attributed to NIPAM in RFPEI, we determined the actual NIPAM/EI molar ratio, which is summarized in Table 1. As indicated in Table 1, when the NIPAM/EI dosage was below 4/5, the measured NIPAM/EI ratio in RFPEI was slightly lower but still close to the theoretical value. However, when the NIPAM/EI dosage reached 5/5, the observed NIPAM/EI ratio was only 4.2/5. This discrepancy could be due to the increased steric hindrance caused by the presence of a side chain in PEI. The hindrance might have impeded the secondary addition of certain imines, leading to a lower measured ratio.

The ^{13}C-NMR spectra (Fig. 1) provides additional insights into the preparation process of RFPEI. In the PEI spectrum (Fig. 1d), eight peaks ranging from 37.8 ppm to 56.1 ppm are observed (Fig. S2 and Table S3 in ESI). These peaks result from the presence of branched chains in PEI, where the methylene group is connected to different nitrogen atoms in distinct microenvironments.[42] When the methylene group is linked to tertiary amine (C1^a, C1^b and C1^c), its peaks appear at higher chemical shifts. However, as more secondary and primary amines are connected, the peaks of the methylene group gradually shift towards lower chemical shifts (refer to Fig. S2 and Table S3 (in ESI) for specific peak chemical shifts). NIPAM exhibits five peaks (Fig. 1e and Table S2 in ESI). The peak corresponding to methyl (C9) appears at 21.3 ppm, methylate (C8) at 41.8 ppm, and the peaks corresponding to the double bonds occur at 126.8 ppm (C4) and 130.3 ppm (C5) due to their connection with the amide group. Additionally, a typical carbonyl carbon peak at 167.3 ppm (C6) is observed.[32,43,44] In the P4 spectrum (Fig. 1f and Table S2 in ESI), the peaks (C8 and C9) attributed to the isopropyl group present in NIPAM, as well as the peaks corresponding to the methylene group in PEI, remain unchanged in terms of chemical shift. However, after the addition reaction between PEI and NIPAM, the peaks associated with the double bond originally assigned to NIPAM disappear. Instead, two new methylene groups appear at 35.6 ppm (C5) and 41.8 ppm (C4), respectively.[32] The positions of C4 and C8 overlap, resulting in a significant increase in the observed peaks in that region. Due to the addition reaction between the amine group and partial imine, the methylene peaks (C2^c, C2^d) related to primary amine present in PEI shift to higher fields and eventually disappear. Simultaneously, the peak corresponding to the methylene groups (C1, C2) connected to secondary amine significantly decreases. Additionally, as the double bond with the carbonyl group transitions to a single bond, the characteristic peak of the carbonyl group shifts from 167.3 ppm to 173.3 ppm.

The FTIR spectra presented in Fig. S3 (in ESI) provide confirmation that the reaction between PEI and NIPAM proceeded successfully. In the spectrum of PEI, the absorption band observed at 3374 cm^{-1} corresponds to the NH_2/NH stretching vibration, while the band at 2958 cm^{-1} is attributed to the methylene stretching vibration absorption. For NIPAM, distinct bands are visible at 3296, 1659 and 1549 cm^{-1}, representing the NH stretching vibration, C=O stretching vibration, and NH bending vibration, respectively. Additionally, a frequency doubling band of the NH bending vibration and band of C=C—H stretching vibration are observed at 3072 cm^{-1}.[32,41,45] These absorption bands mentioned above are also evident in the RFPEI spectrum, albeit with some displacement due to the changes in the chemical environment. Notably, the stretching vibration absorption band of the C=C group at 1618 cm^{-1} presented in NIPAM is not observed in RFPEI (P4), providing confirmation of the occurrence of an aza-Michael addition reaction between NIPAM and PEI. Furthermore, the wide bands observed at 3200 cm^{-1} to 3500 cm^{-1} in P4 indicate the presence of the amide group and amine/imine stretching vibrations. The bands at 2800 cm^{-1} to 2980 cm^{-1} can be attributed to the $-CH_3$ and $-CH_2-$ groups.

Additionally, the M_n and PDI of RFPEI were determined through GPC, with the results listed in Table 1. It is observed that as the NIPAM/EI ratio increases, more amine/imine groups in PEI react with NIPAM, leading to an increase in M_n. M_w increases more than M_n, and number of PEI molecular chain remains unchanged. Furthermore, it is different of the addition ratio of NIPAM to each PEI molecular chain, resulting in increased PDI with the NIPAM/EI ratio increasing. These findings collectively demonstrate that the aza-Michael addition reaction between PEI and NIPAM proceeded smoothly, resulting in the successful synthesis of RFPEI.

LCST and UCST of RFPEI

LCST-type polymers undergo a transition from a dissolved free chain state to a curly state as the temperature increases, leading to precipitation. On the other hand, UCST-type polymers are soluble at high temperatures but become insoluble below the critical temperature.[33,35] RFPEI demonstrates both LCST and UCST responsiveness, with its LCST being smaller than UCST. This means that it exhibits hydrophobic behavior at intermediate temperatures and hydrophilic behavior at temperatures below the LCST (<30 °C) and above the UCST (>80 °C) (Fig. S4 in ESI). These temperature-induced transitions in RFPEI's solubility are governed by the competitive relationship between polymer molecules and between the polymer and solvent molecules.[35] At temperatures between the LCST and UCST, the interaction between RFPEI polymer chains becomes stronger than the interaction between the polymer chains and water molecules, resulting in the aggregation and contraction of the polymer chains and a turbid solution. As the temperature decreases below the LCST, the hydrogen bonding between RFPEI and water strengthens, forming a hydration layer on the polymer chain, leading to dissolution of the polymer. Increasing the temperature to the UCST point reduces intermolecular and intramolecular forces, but the thermal motion of the polymer chains and water increases, increasing the polymer's solubility and causing it to dissolve in water again, resulting in a clear solution.[46]

The effects of the NIPAM/EI ratio on the hydrophilic proper-

ties of RFPEI were examined by evaluating the temperature-dependent light transmittance of polymer aqueous solutions (P1–P5) at different concentrations (25.0, 50.0, 75.0, and 100.0 mg/mL, Fig. 2a and Fig. S5 in ESI). When the NIPAM/EI molar ratio was low (1/5, P1), the solution remained clear and transparent across the entire observed temperature range (20–80 °C) at any concentration. This indicated that P1 did not exhibit temperature responsiveness. However, as the NIPAM/EI ratio continuously increased from 2/5 to 5/5, the light transmittance of the polymer (P2–P5) initially decreased (LCST) and then increased (UCST) with an increase in temperature. This trend became more prominent as the NIPAM/EI ratio increased. For instance, at a concentration of 50.0 mg/mL, the transmittance of P2 only decreased to 90% with temperature rise, while P3, P4 and P5 had lower transmittances of 45%, 17% and 8%, respectively. This indicated that the higher NIPAM/EI ratios resulted in a greater change in light transmittance with temperature variation.

PEI is a hydrophilic polymer, and its aqueous solution remains clear and transparent within the observed range (20–80 °C). The isopropyl amides are the key groups for the LCST-type temperature responsiveness of poly(NIPAM).[19,34] The LCST behavior of RFPEI arises from the changing interaction between the isopropyl amides and water molecules at different temperatures. At lower temperatures, the isopropyl amides can form hydrogen bonds with water, leading to the formation of a hydration layer around the RFPEI chains. This hydration layer enhances the hydrophilicity of RFPEI and allows it to remain soluble in water. As the temperature increases, the strength of the hydrogen bond interactions decreases. Once the temperature reaches the LCST value, the force of the hydrogen bonds between the polymer and water becomes weaker than the polymer-polymer interactions. Consequently, RFPEI undergoes a transition from a hydrophilic state to a hydrophobic state, causing it to precipitate out of the aqueous solution. The increase in the isopropyl amide content within RFPEI leads to a more significant effect on this transition. As a result, the changes in transmittance become more pronounced with an increase in the NIPAM/EI ratio, as depicted in Fig. S5 (in ESI).

In the study, the LCST and UCST values were specified when the transmittance of an aqueous polymer solution reached 50%. For P2, although its transmittance changed with temperature, it did not decrease to 50% within the observed range. Therefore, the specific LCST and UCST values of P2 were not recorded. When the polymer was at a concentration of 50.0 mg/mL, the LCST value of the polymer decreased as the NIPAM/EI ratio increased. and the LCST values of P3, P4 and P5 were found to be 41.0, 36.7 and 35.4 °C, respectively (Table S4 in ESI). It is commonly known that for hydrophilic group-included LCST-type polymers, the LCST value typically increases. Conversely, the LCST value decreases with the inclusion of hydrophobic groups.[30,32,33] In this case, as more NIPAM is introduced, the hydrophilic EI unit in RFPEI decreases, resulting in diminished hydrophilic properties of RFPEI. Consequently, the LCST value of the polymer decreases.

Based on Fig. 2(a), Fig. S5 and Table S4 (in ESI), it is evident that the UCST value of RFPEI increases with an increase in the NIPAM/EI ratio at the same concentration. Taking the example of a concentration of 50.0 mg/mL, the UCST values of P3, P4 and P5 are 50.3, 63.9 and 71.0 °C, respectively. Neat PEI, which contains only hydrophilic EI units, exhibits smaller intermolecular forces compared to the interaction between molecular chains and water. As a result, it remains clear and transparent over the observed temperature range. However, when NIPAM was introduced, the carbonyl groups form hydrogen bonds with amine/imine groups, and there is a hydrophobic interaction between NIPAM within the temperature range from LCST to UCST. This leads to significantly enhanced intermolecular and intramolecular interactions. To counteract this effect under the same conditions, a higher temperature is required. Therefore, the UCST value of the polymer increases as the NIPAM/EI ratio increases.

The phase transition temperature of RFPEI is influenced by the concentration of the polymer.[30,32] At a low concentration of 25.0 mg/mL (Fig. S5a in ESI), the light transmittance of P2–P5 aqueous solution initially decreased and then increased with increasing temperature. However, the light transmittance of all samples did not drop to 50%, so we did not record the LCST and UCST. As the polymer concentration increased, the LCST value of RFPEI decreased while the UCST value increased. Considering the example of P4 (Fig. S5 and Table S4 in ESI), when the concentration increased from 50.0 mg/mL to 100.0 mg/mL, its LCST decreased from 36.7 °C to

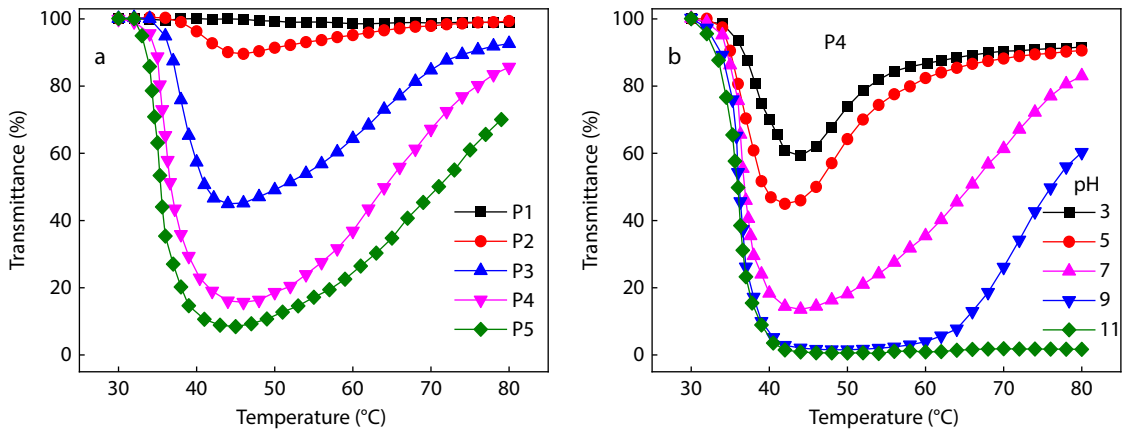

Fig. 2 Temperature-dependent light transmittance spectra (600 nm) of aqueous solution of RFPEI (P1–P5) at 50.0 mg/mL and pH 7 (a), and that of P4 at varied pH values with fixed concentration of 50.0 mg/mL (b).

https://doi.org/10.1007/s10118-024-3120-x

35.0 °C, and its UCST increased from 63.9 °C to 71.1 °C. This behavior can be explained by the increase in the number of molecular chains per volume as the polymer concentration increases. With a higher concentration, there is a greater probability of interaction between the molecular chains. The increased interchain forces require more hydrogen bonding forces between RFPEI chains and water molecules to counterbalance each other. Consequently, the temperature required to achieve force equilibrium between polymer- polymer and polymer-H_2O interactions is reduced, resulting in a decrease in the LCST. Similarly, in hot regions (for UCST), higher temperatures are needed to further reduce the concentration-enhanced polymer-polymer force by thermal motion of H_2O molecules. Overall, the influence of polymer concentration on the phase transition temperature of RFPEI is attributed to the increased interchain forces and subsequent changes in the equilibrium between polymer- polymer and polymer-H_2O interactions at different temperatures.

The temperature-dependent light transmittance of RFPEI solution (50.0 mg/mL) at different pH values is shown in Fig. 2(b) and Fig. S6 (in ESI) (P2–P5). The corresponding LCST and UCST values are listed in Table S5 (in ESI). When the pH value is not higher than 9, the transmittance of the RFPEI aqueous solution initially decreases and then increases with increasing temperature. This change trend is relatively weak at low pH values but becomes more pronounced as the pH value increases. For example, when pH=3, the light transmittance of P4 is only reduced to 60%. However, when the pH is above 9, the light transmittance can be reduced to less than 2%. Furthermore, as the pH value increases, the LCST of RFPEI decreases gradually while the UCST increases. Taking P4 as an example again, the LCST decreases from 39.5 °C at pH=5 to 35.7 °C at pH=11. Similarly, the UCST increases from 45.8 °C at pH=5 to 76.0 °C at pH=9. No UCST was observed within the detection range when the pH value was further increased to 11. These results depend on the different states of amine/imine groups in the molecular chains under varying pH values. At lower pH values, amine/imine protolysis occurs ($-NH_3^+/=NH_2^+$), which enhances the interaction between RFPEI and water, making RFPEI more hydrophilic. Additionally, the electrostatic repulsion between ionized RFPEI also increases, weakening the interaction between RFPEI chains. As a result, the polymer is less likely to precipitate from the water, leading to a weaker change in light transmittance, as well as higher LCST and lower UCST values. On the other hand, at higher pH values, amine/imine deprotonation ($-NH_2/=NH$) reduces the hydrophilicity of RFPEI and weakens the electrostatic repulsion between polymer chains. This leads to lower LCST values and higher UCST values.

Fluorescence Property of RFPEI

As shown in Fig. S4(b) (in ESI), the RFPEI aqueous solution (50.0 mg/mL) exhibits bright blue fluorescence under ultraviolet irradiation, with its fluorescence properties changing at different temperatures. The optimal excitation (λ_{ex}) and emission (λ_{em}) wavelengths of P0–P5 aqueous solutions (50.0 mg/mL, pH=7, 25 °C) were determined (Fig. S7 and Table S6 in ESI). It is evident that the fluorescence intensity (FI) and λ_{em} of RFPEI are closely related to the NIPAM/EI ratio. Under the same conditions, the FI of PEI (P0) is very weak (lower than 40), whereas the FI of other samples is stronger (Fig. S7 in ESI). Previous literatures reported that the presence of amide-amine groups as fluorophores.[47,48] Therefore, we believe that the fluorescence of RFPEI originates from the formation of amide-amine groups following the addition of NIPAM to PEI. As the NIPAM/EI ratio increases, more amide-amine groups are formed, resulting in a sharp increase in FI for P1 and P2. However, as the NIPAM/EI ratio further increases, although more amide-amines are formed, the amine/imine groups in RFPEI decrease. This reduction weakens the hydrogen bond between the amine/imine and amide-amine groups, which hinders the formation of intra- and/or inter-molecular clusters, leading to a slight decrease in FI from P3 to P5. To validate the impact of amide-amine interactions on the fluorescence enhancement, the fluorescence emission spectra of PEI, free NIPAM and their fresh mixture solution were compared with P4 at the equivalent concentration (50.0 mg/mL, λ_{ex}=370 nm, Fig. S8 in ESI). It can be seen that, free NIPAM and its mixture with PEI also have fluorescence emission, and the fluorescence spectrum of the mixture is similar to that of NIPAM. However, their λ_{em} are all at 432 nm, which is very different from the 480 nm of P4. Thus, it can be inferred that the fluorescence emission of RFPEI comes from the amide-amine groups formed after the addition of NIPAM and PEI, rather than their non-covalent complexes. Furthermore, a certain volume of hexafluoroisopropanol (1.0 vol%–4.0 vol%), a hydrogen bonding destroying agent, was added into P4 aqueous solution (50.0 mg/mL), and the fluorescence emission spectra excited at 370 nm were determined (Fig. S9 in ESI). With the increase of hexafluoroisopropanol content, the fluorescence intensity of P4 decreased significantly at first and then slowly, that may be because that the hydrogen bond interaction between P4 molecules was destroyed by adding hexafluoroisopropanol. Additionally, as the NIPAM/EI ratio increases, the optimal λ_{em} shifts from 467 nm for P1 to 475 nm for P5 (Table S6 in ESI).

The fluorescence emission spectra of RFPEI (P0–P5) aqueous solution (50.0 mg/mL, pH=7, 25 °C) at different λ_{ex} were recorded (Fig. 3a and Fig. S10 in ESI). With increasing λ_{ex}, the FI of RFPEI (P1–P5) aqueous solution initially increases and then decreases, while the λ_{em} red-shifts accordingly. This indicates that RFPEI exhibits excitation-dependent fluorescence emission. In studies of CTE polymers, size effect has been the widely accepted theory for excitation dependent emission, *i.e.*, the energy gaps are determined by the size of the localized C=O clusters and their size distribution, and emission is determined by this band gap. The smaller is the size, the wider is the energy gap.[25,28] The fact that RFPEI emission had excitation dependent property was exactly because clusters of different size were formed. The FI of P1–P5 reaches its maximum at an excitation wavelength of 370 nm, thus 370 nm is selected as the optimal λ_{ex} under these conditions (50.0 mg/mL, pH=7) for further study.

The FI of CTE polymers is closely related to the polymer concentration.[23,25,28,30] To investigate this relationship, the fluorescence spectra of RFPEI (P1–P5) were measured at different concentrations using an excitation wavelength of 370 nm (Fig. 3b and Fig. S11 in ESI). The results show that the FI of RFPEI aqueous solution initially increased and then decreased with increasing polymer concentration. For all samples (P1–P5), the FI reached its maximum at a concentration

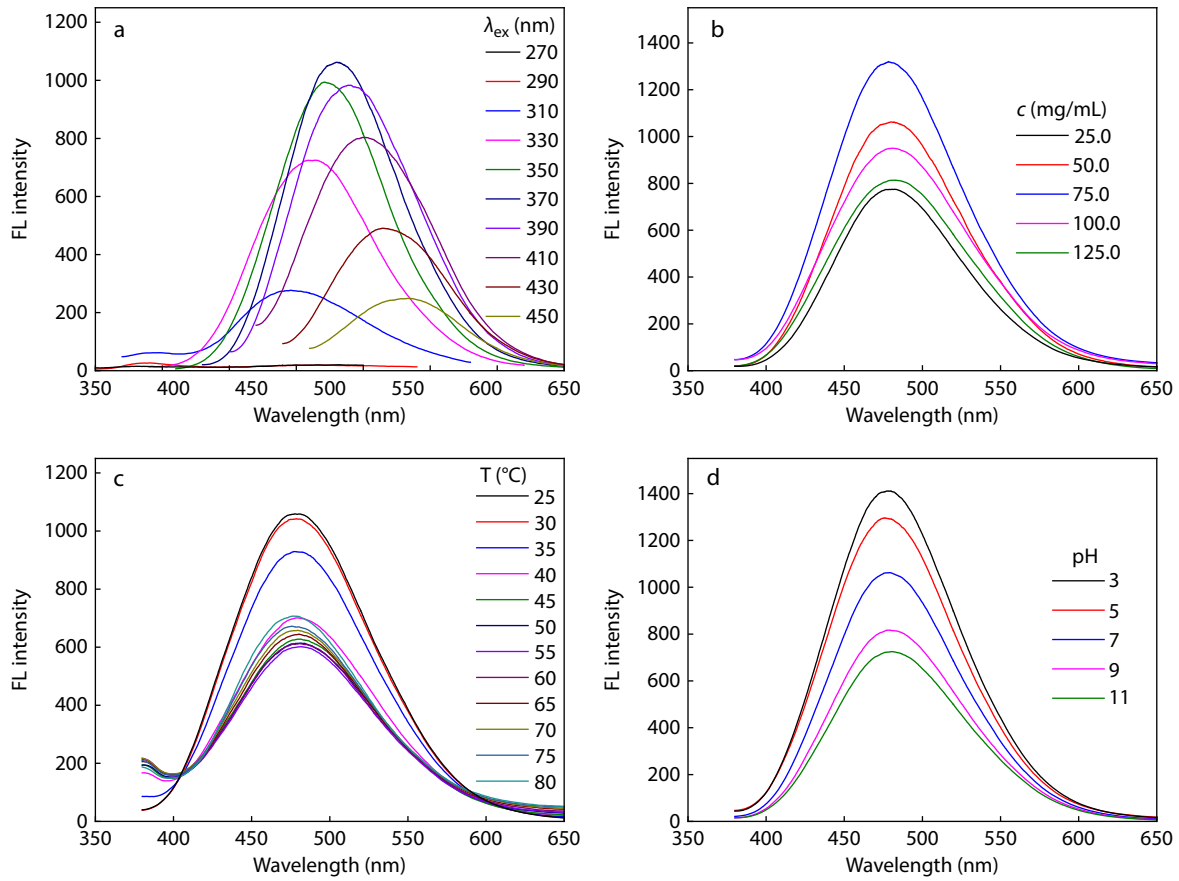

Fig. 3 Fluorescence emission spectra of P4 aqueous solution at different excitation wavelengths (a, 50.0 mg/mL, pH 7, 25 °C); and that at different concentrations (b, 25 °C, pH=7), different temperatures (c, 50.0 mg/mL, pH=7) and different pH (d, 50.0 mg/mL, 25 °C) all excited at 370 nm.

of 75.0 mg/mL. This observation may be attributed to changes in the clustering state of RFPEI at different concentrations, leading to variations in its optimal excitation wavelength (λ_{ex}). To further support this hypothesis, we examined the excitation dependence of P4 at different concentrations (Fig. S12 and Table S7 in ESI). The results indicated that, regardless of the concentration, the emission wavelength (λ_{em}) of P4 aqueous solution increased as the λ_{ex} increased, and the FI exhibited an initial increase followed by a decrease. Specifically, when the P4 concentration was not higher than 75.0 mg/mL, the FI was maximized at an excitation wavelength of 370 nm. However, when the P4 concentration reached 100.0 mg/mL, the FI was maximized at an excitation wavelength of 390 nm.

The cluster state of polymers in solution is dependent on temperature.[28,30] Thus, we detected the fluorescence emission spectra of RFPEI aqueous solution (50.0 mg/mL, pH=7) at different temperatures (Fig. 3c and Fig. S13 in ESI). As mentioned earlier, P1 did not show any thermo-responsive behavior and remained clear and transparent within the observed temperature range (Fig. S5 in ESI). The increase in temperature aggravates the movement of polymer molecules, which is not favorable for the formation of clusters. Therefore, FI of P1 gradually decreases with increasing temperature (Fig. S13a in ESI). On the other hand, the FI of P2–P5 initially decreases and then increases with temperature, accompanied by a rapid decrease in FI at 30–45 °C (Figs. S13b–S13e in ESI). This can be attributed to the sharp decrease in light transmittance of the RFPEI solution at 30–45 °C, where the turbid solution scatters part of the exciting light, thereby obstructing its penetration into the solution. The change in light transmittance of P2 is less significant compared to that of P3–P5 (Fig. S5 in ESI), resulting in a less significant reduction in FI for P2 between 30 and 45 °C. When the temperature exceeds 65 °C, the FI starts to increase (Fig. S13f in ESI). This is because the temperature reaches the UCST of RFPEI, causing the solution to become clear and transparent. However, such high temperatures are not conducive to the formation of polymer clusters, hence the FI is much lower than those of clarified transparent aqueous solutions at lower temperatures (<LCST). For P4 at a low concentration (5.0 mg/mL), there is slight change in light transmittance (Fig. S14a in ESI), hence no sudden reduction in FI can be observed (Fig. S14b and S14c in ESI). From the above description, it can be seen that for temperature-responsive polymers, FI is influenced by temperature in two ways. First, the increase in temperature enhances the movement of polymer molecules, disrupting cluster formation and reducing FI. Second, the change in light transmittance of the solution with temperature affects the permeation of exciting light into the solution, leading to a reduction in FI.

The protonation-deprotonation of amine/imine groups in polymers, which occurs at different pH values, leads to the formation of distinct clustering states.[28,30] The fluorescence emission spectra of RFPEI aqueous solution (50.0 mg/mL)

https://doi.org/10.1007/s10118-024-3120-x

were recorded at various pH values using an excitation wavelength of 370 nm. As shown in Fig. 3(d) and Fig. S15 (in ESI), the FI of RFPEI gradually decreases with an increase in pH value. The most significant decrease in FI occurs within the pH range of 5–7, where the amines undergo protonation or deprotonation. It should be noted that for some amine-containing polymers, the protonated amine groups make the polymers more hydrophilic, which is not favorable for the CTE property.[28,49] In contrast to these amine-containing polymers, RFPEI exhibits higher FI at low pH values, and this phenomenon can be attributed to two reasons. First, the charged amine/imine groups reposition themselves towards the periphery of the molecular clusters, causing the amide-amine groups to stack more tightly within the clusters and limiting the free rotation of the polymer chain to some extent. Second, the charged amine/imine groups also participate in the aggregation of amide-amine groups, resulting in an increased charge density and enhanced fluorescence.

Emission Mechanism of RFPEI

It is generally believed that, the formed polymer clusters are the source of CTE, and its clustering state is affected by polymer concentration, temperature, pH, and so on, resulting in fluorescence changes.

DLS was employed to analyze the cluster size and size distribution of RFPEI aqueous solutions at different concentrations (pH=7) (Fig. 4a, Fig. S16 and Table S8 in ESI). The results indicate that the cluster size of RFPEI slightly decreases with increasing polymer concentration up to 75.0 mg/mL. However, beyond this concentration, the cluster size sharply increases.

Taking P4 as an example (Fig. 4a), its cluster size decreases slightly from 2.09 nm to 1.49 nm as the concentration increases from 25.0 mg/mL to 75.0 mg/mL. But when the concentration reaches 100.0 mg/mL and 125.0 mg/mL, the cluster size rapidly increases to 58.36 and 99.05 nm, respectively. This abrupt change in cluster size is consistent with the corresponding FI changes observed with varying P4 concentrations (Fig. 3b). Interestingly, it is worth noting that RFPEI exhibits the smallest cluster size and the largest FI (λ_{ex}=370 nm) at a concentration of 75.0 mg/mL. In contrast to previous studies where FI of polymers and their cluster size increase with polymer concentration,[23,28,30] our findings reveal an inverse relationship for RFPEI. This can be attributed to the fact that smaller clusters have a more compact structure and higher electron cloud density.

Furthermore, we investigated the cluster size of RFPEI aqueous solution (50.0 mg/mL) at different pH values (Fig. 4b, Fig. S17 and Table S9 in ESI). It can be observed that the cluster size of RFPEI gradually increases as the pH value increases. For instance, the cluster size of P4 increases from 1.28 nm at pH=3 to 3.30 nm at pH=11 (Fig. 4b). As discussed earlier, the FI reaches the strongest at lower pH values and the weakest at higher pH values (Fig. 3d). Moreover, it is still inversely pro-

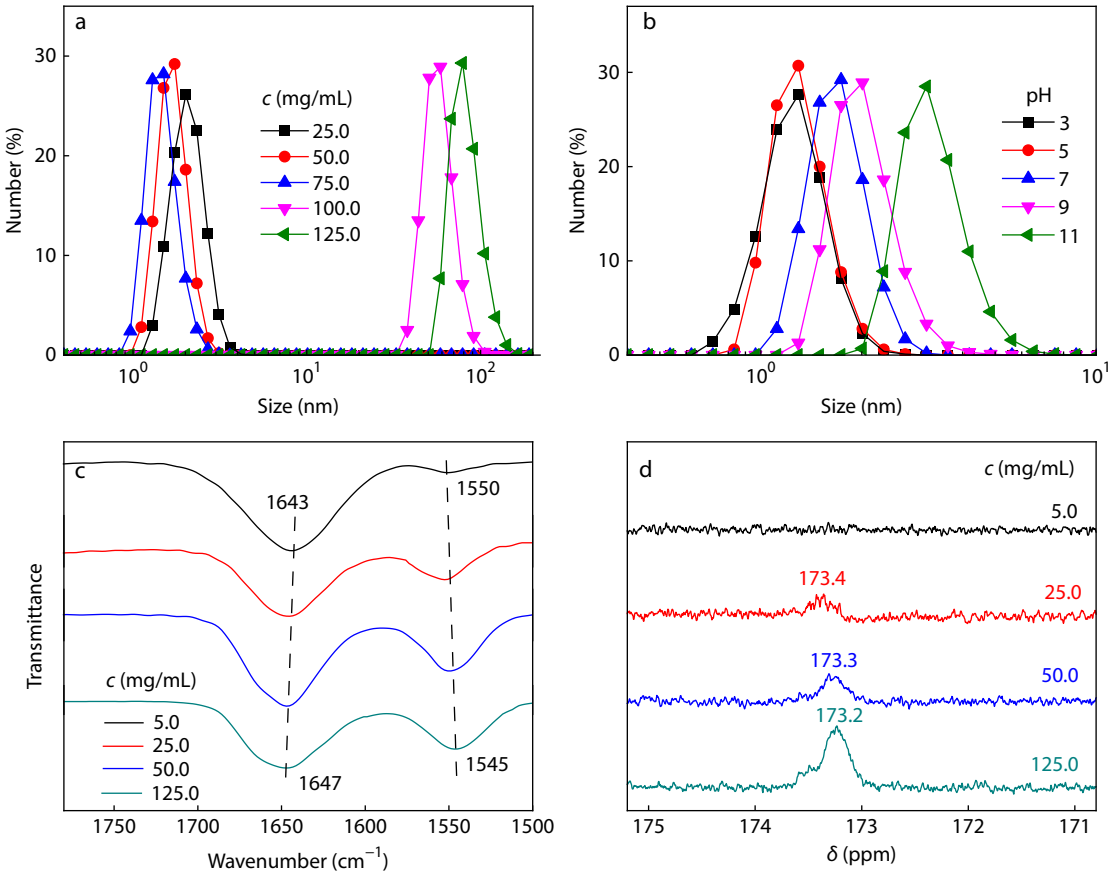

Fig. 4 Particle size distribution of P4 aqueous solution at different concentrations (a, pH=7, 25 °C) and that at different pH (b, 50.0 mg/mL, 25 °C); FTIR (c) and ^{13}C-NMR (d) of P4 at different concentrations.

https://doi.org/10.1007/s10118-024-3120-x

portional to the particle size. This observation indirectly supports the hypothesis that the charged amine/imine group flips to the periphery of the cluster, causing the fluorescence-producing amide-amine groups to be more densely packed inside the clusters.

Moreover, FTIR and NMR are also reliable techniques to confirm the formation of clusters.[23–30] In the case of P4 aqueous solution, FTIR and ^{13}C-NMR were conducted at different concentrations (Figs. 4c and 4d). When the concentration of P4 increased from 5.0 mg/mL to 125.0 mg/mL, notable changes can be observed in the FTIR spectra. Specifically, the stretching vibration band of the C=O bond shifts from 1643 cm^{-1} to 1647 cm^{-1}, while the bending vibration band of the NH group shifts from 1550 cm^{-1} to 1545 cm^{-1} (Fig. 4c). Furthermore, when the concentration of P4 increased from 5.0 mg/mL to 125.0 mg/mL, the chemical shift of the C=O bond altered from 173.4 ppm to 173.2 ppm in the ^{13}C-NMR spectrum (Fig. 4d). This can be attributed to the movement of electrons from the NH bond towards the C=O group as the concentration of P4 increases. Consequently, the electron cloud density around the C=O group increases, whereas it decreases around the NH bond.[28,30]

Cell Imaging, Trace Detection and Controlled Release of DOX

The cytotoxicity of RFPEI (P4) was assessed using a standard MTT assay (details are shown in ESI). 4T1 cells were treated with P4 at a concentration of 0–20.0 μg/mL for 24 h, and the results showed a high cell viability of 97% (Fig. S18 in ESI), indicating that P4 has low cytotoxicity towards 4T1 cells. Subsequently, the cells were incubated with the same concentration of P4 (10.0 μg/mL) for 24 h and observed under confocal microscopy. The images show blue and green fluorescence signals (Fig. 5), indicating that P4 can easily entered living cells. Furthermore, the probe was mainly localized in the cytoplasm, which overlapped perfectly with the fluorescent distribution in the merged images. These findings suggest that P4 has the potential to be used for bio-imaging purposes.

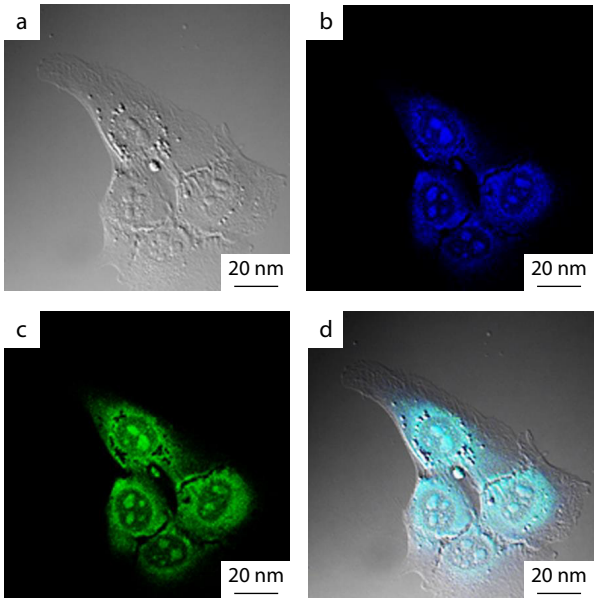

Fig. 5 Confocal fluorescence images of living 4T1 cells with excitation at 405 nm after incubation in presence of P4 (10.0 μg/mL) for 24 h: (a) bright filed, (b) blue channel (425–475 nm), (c) green channel (500–550 nm), (d) merged image.

UV spectra show that DOX (40 μmol/L) and P4 solution have no absorption at 600 nm (Fig. S19 in ESI), thus the added DOX in RFPEI solution did not interfere with the measurement of LCST and UCST. The effect of DOX concentration (defined as [DOX], μmol/L) on LCST and UCST of RFPEI (50.0 mg/mL) was tested (Fig. S20 and Table S10 in ESI). With the increase of [DOX], LCST of RFPEI gradually decreases and UCST increases. Taking P4 for example, with [DOX] increases from 0 μmol/L to 120 μmol/L, LCST decreases from 37.8 °C to 36.1 °C, and UCST increases from 62.5 °C to 68.6 °C. When hydrophobic DOX is added into RFPEI, the RFPEI-DOX complexes are formed through hydrogen bond interaction. The formed RFPEI-DOX is more hydrophobic than RFPEI, thus the LCST decreases and UCST increases.

The optimal λ_{ex} and λ_{em} of DOX aqueous solution (100 μmol/L) are 502 and 568 nm, respectively (Fig. S21a in ESI). Additionally, there is minimal emission at 568 nm when excited at 370 nm (Fig. S21b in ESI), indicating that the intrinsic emission of DOX has negligible influence on RFPEI emission. To evaluate the impact of DOX concentration on RFPEI emission, we recorded the fluorescence spectra of RFPEI aqueous solution (50.0 mg/mL) with different [DOX] (Fig. 6a and Fig. S22 in ESI, λ_{ex}=370 nm, 0–100 μmol/L). As [DOX] increases, the emission peak of RFPEI undergoes a blue shift and the fluorescence intensity gradually decreases. Simultaneously, new peaks appear in the range of 550–600 nm, which can be attributed to the emission of DOX. In Fig. S21(a) (in ESI), it is evident that DOX emits within the range of 550–600 nm when excited at 502 nm, and the emission spectrum of RFPEI (P4) coincides with the excitation spectrum of DOX within the range of 400–550 nm. The UV spectrum of DOX (Fig. S19 in ESI) also confirms its strong absorption peak within this range. Hence, the fluorescence quenching mechanism of RFPEI by DOX is apparent, whereby the emission of RFPEI is absorbed by DOX. Some literatures refer to it as inner filter effect.[30,49,50]

The blue shift observed in RFPEI emission wavelength when mixed with DOX is partially caused by the decrease in electron cloud density of the carbonyl and NH groups on RFPEI. This can be supported by FTIR spectra of RFPEI mixed with varying content of [DOX] (Fig. S23 in ESI). Specifically, the stretching vibration band of the C=O group red shifts from 1645 cm^{-1} to 1642 cm^{-1}, and the bending vibration band of NH red-shifts from 1549 cm^{-1} to 1544 cm^{-1} when [DOX] in the mixed solution increases from 0 μmol/L to 20 μmol/L. Moreover, the stretching vibration band of NH_2/NH (3466 cm^{-1}) gradually decreases. These results indicate that the RFPEI-DOX complexes are formed through hydrogen bond interaction.

When the concentration of DOX is in the range of 2–10 μmol/L, FI of RFPEI decreases linearly with increasing DOX concentration (Fig. 6b). The detection limit (DL) was calculated using the equation: $DL = K \times \sigma/S$,[25–27,29,30] where K is a numerical factor (usually taken as 3 for a confidence level of 99.9%), σ is the standard deviation of the blank samples from at least 20 measurements, and S is the slope of the linear

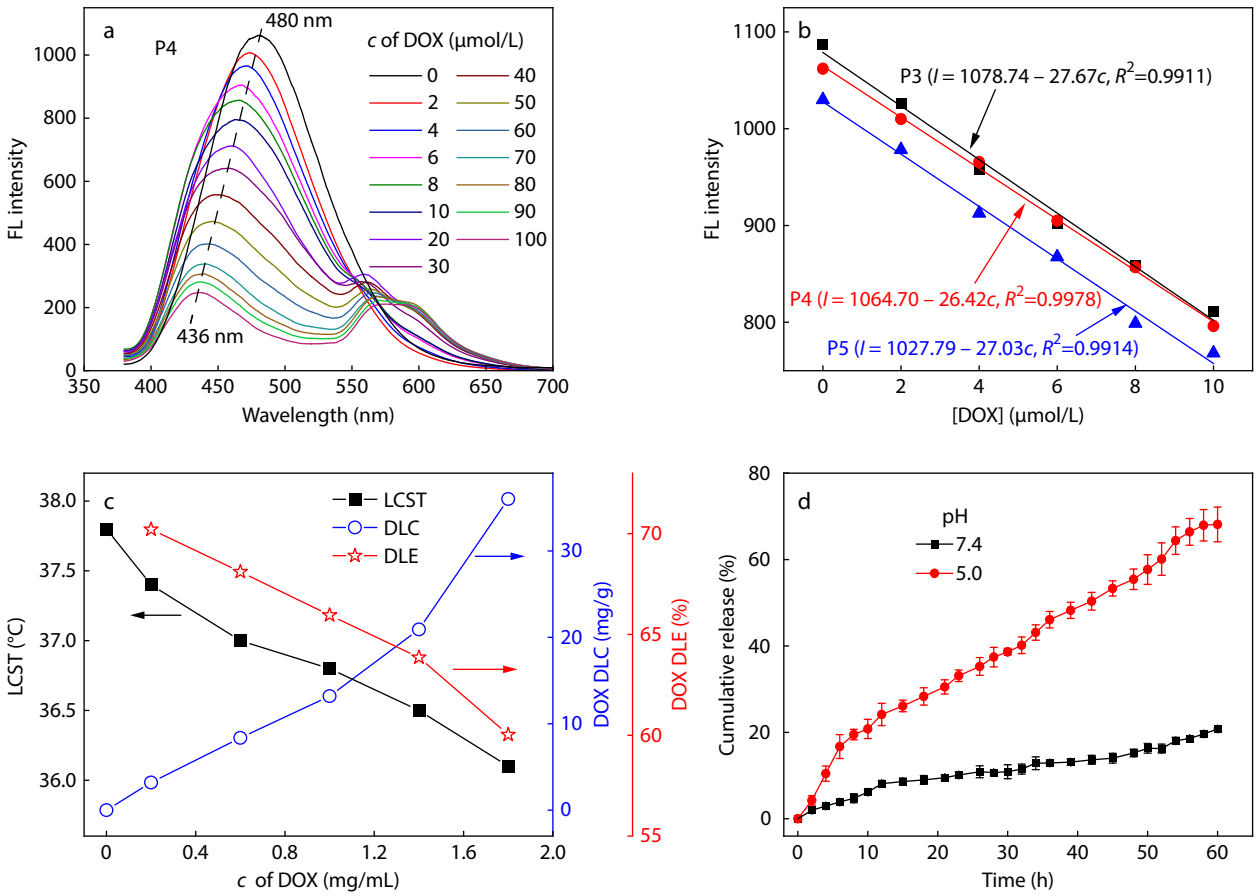

Fig. 6 Fluorescence emission spectra of P4 (50.0 mg/mL) with varied [DOX] (a, 0–100 μmol/L), and linear fitting of fluorescence intensity and [DOX] (b); LCST value (■), DLC (○) and DLE (☆) of DOX-loaded P4 (c, 50.0 mg/mL, pH 7) and cumulative DOX release from the P4 micelles at 37 °C with varied pH (d).

curve of FI versus DOX concentration. The calculated DL values for DOX using P3, P4 and P5 are 2.8×10^{-7} mol/L (σ=2.60, S=27.67), 5.1×10^{-7} mol/L (σ=4.51, S=26.42) and 5.3×10^{-7} mol/L (σ=4.81, S=27.03), respectively. The DL of DOX using RFPEI is better and comparable to the DOX probes reported in the literature (Table S11 in ESI).[51–55] The reported DOX probes with lower DLs are often carbon dots, quantum dots, metal nanoparticles, *etc*., which require complex preparation processes. In this work, RFPEI was prepared in one step through catalyst-free aza-Michael addition of PEI with NIPAM at room temperature, offering a new strategy for preparing DOX probes.

Based on their multi-responsiveness, RFPEI can be used for loading and controlled release of drugs. Since the LCST of P4 is close to the human body temperature, we studied the loading and controlled release behavior of P4 on DOX (details in ESI). At low temperature (25 °C), certain amount of DOX is dissolved in P4 aqueous solution (50.0 mg/mL, pH 7.4). At this time, the polymer chain is in the stretched state, and DOX is easy to produce hydrogen bond interaction with the molecular chain. This interaction has been certified by the changes in LCST (Fig. S20 in ESI) and characteristic bands in FTIR spectra (Fig. S23 in ESI). Once the temperature reaches up to 37 °C, P4 with DOX are coprecipitated from solution and micelles with DOX core and P4 shell are formed with particle size about 4.2 nm (Fig. S24 in ESI). The unloaded DOX is separated by dialysis method and its concentration in phosphoric acid buffer outside the dialysis tube is calculated by DOX standard curve (Fig. S25 in ESI). Load capacity (DLC, mg/g) and load efficiency (DLE, %) of DOX by P4 were recorded at varied added amount of DOX (Fig. 6c). With added DOX increases, the DLC increases and DLE decreases. When 1.0 mg/mL DOX is added, DLC of DOX by P4 is 13.19 mg/g and DLE is 65.96 %.

The DOX loaded P4 (DLC=13.19 mg/g, DLE=65.96%) in dialysis tube was directly immersed into 150 mL of distilled water, and the cumulative drug release at different time was measured (Fig. 6d). It is clear to see that a gentle release of DOX from P4 micelles was observed at pH 7.4, only 20% DOX is released after 60 h. However, a rapid release of DOX is observed at pH 5.0 (Fig. 6d) and around more than 68% DOX is released after 60 h. Thus, P4 is potential in pH-induced drug release.

CONCLUSIONS

In this study, a multi-responsive polymer RFPEI was prepared between PEI and NIPAM using a non-catalytic aza-Michael addition reaction and its structure was thoroughly characterized. The polymer exhibits both LCST and UCST properties in water. The influence of the NIPAM/EI molar ratio, polymer concentra-

https://doi.org/10.1007/s10118-024-3120-x

tion, pH, and temperature on the phase transition behavior was investigated. It was found that at P4 concentration of 50.0 mg/mL and pH 7, the LCST of P4 was 36.7 °C, which closely resembles human body temperature. Additionally, the effect of temperature, pH, and concentration on the fluorescence properties of the polymer was examined and correlated with the phase transition process. The luminescence mechanism was elucidated through various techniques, including DLS, FTIR, and NMR, revealing that it is based on the formation of copolymer clusters through the interaction of amide-amine groups and imine groups. Finally, the potential applications of RFPEI in cell imaging, controlled release of DOX, and trace detection were demonstrated. The utilization of RFPEI in antitumor drug delivery systems holds great significance in research endeavors.

Conflict of Interests

The authors declare no interest conflict.

Electronic Supplementary Information

Electronic supplementary information (ESI) is available free of charge in the online version of this article at http://doi.org/10.1007/s10118-024-3120-x.

Data Availability Statement

The data that support the findings of this study are available from the corresponding author upon reasonable request. The authors' contact information: chm_zhuxl@ujn.edu.cn (X.L.Z.), chm_liss@ujn.edu.cn (S.S.L.).

ACKNOWLEDGMENTS

This work was financially supported by Nature Science Foundation of Shandong Province, China (Nos. ZR2021MB112 and ZR2022MB051), Science and Technology Bureau of Jinan City (2021GXRC105), Postdoctoral Science Foundation of China (2022M712343), as well as by Basic and Applied Basic Research Foundation (2020A1515110374) of Guangdong Province, China.

REFERENCES

1 Zhang, J.; He, B.; Hu, Y.; Alam, P.; Zhang, H.; Lam, J. W. Y.; Tang, B. Z. Stimuli-responsive AIEgens. *Adv. Mater.* **2021**, *33*, 2008071.
2 Li, J.; Du, N.; Tan, Y.; Hsu, H. Y.; Tan, C.; Jiang, Y. Conjugated polymer nanoparticles based on copper coordination for real-time monitoring of pH-responsive drug delivery. *ACS Appl. Bio Mater.* **2021**, *4*, 2583–2590.
3 Pooresmaeil, M.; Namazi, H.; Salehi, R. Dual anticancer drug delivery of D-galactose-functionalized stimuli-responsive nanogels for targeted therapy of the liver hepatocellular carcinoma. *Eur. Polym. J.* **2022**, *167*, 111061.
4 Xiao, Y.; Pandey, K.; Nicolás-Boluda, A.; Onidas, D.; Nizard, P.; Carn, F.; Lucas, T.; Gateau, J. m.; Martin-Molina, A.; Quesada-Pérez, M.; Ramos-Tejada, M. D. M.; Gazeau, F.; Luo, Y.; Mangeney, C. Synergic thermo- and pH-sensitive hybrid microgels loaded with fluorescent dyes and ultrasmall gold nanoparticles for photoacoustic imaging and photothermal therapy. *ACS Appl. Mater. Interfaces* **2022**, *14*, 54439–54457.
5 Zhang, P.; Xue, M.; Lin, Z.; Yang, H.; Zhang, C.; Cui, J.; Chen, J. Aptamer functionalization and high-contrast reversible dual-color photoswitching fluorescence of polymeric nanoparticles for latent fingerprints imaging. *Sensor Actuat. B* **2022**, *367*, 132049.
6 Sha, H.; Yan, B. A pH-responsive Eu(III) functionalized metal-organic framework hybrid luminescent film for amino acid sensing and anti-counterfeiting. *J. Mater. Chem. C* **2022**, *10*, 7633–7640.
7 Yu, Y.; Si, M.; Lu, W.; Wu, S.; Wei, S.; Wu, B.; Chen, X.; Xie, W.; Chen, T. Confining monochromophore in dynamic polymer network for multi-stimuli responsive fluorescence-phosphorescence dual-emission. *Chem. Eng. J.* **2023**, *478*, 147271.
8 Moniruzzaman, M.; Kim, J. N-doped carbon dots with tunable emission for multifaceted application: solvatochromism, moisture sensing, pH sensing, and solid state multicolor lighting. *Sensor Actuat. B* **2019**, *295*, 12–21.
9 Cheng, Y.; Dai, J.; Sun, C.; Liu, R.; Zhai, T.; Lou, X.; Xia, F. An intracellular H_2O_2-responsive AIEgen for the peroxidase-mediated selective imaging and inhibition of inflammatory cells. *Angew. Chem. Int. Ed.* **2018**, *57*, 3123–3127.
10 Zhang, L.; Zhao, Y.; Kexin Li; Yu, S.; Dong, R.; Ma, S.; Liu, H.; Xing, L.; Zhou, F. Bioinspired simultaneous regulation in fluorescence of AIEgen-embedded hydrogels. *Soft Matter* **2023**, *19*, 7093–7099.
11 Li, B.; He, T.; Shen, X.; Tang, D.; Yin, S. Fluorescent supramolecular polymers with aggregation induced emission properties. *Polym. Chem.* **2019**, *10*, 796–818.
12 Wu, C. H.; Nhien, P. Q.; Cuc, T. T. K.; Hue, B. T. B.; Lin, H. C. Designs and applications of multi-stimuli responsive FRET processes in AIEgen-functionalized and bi-fluorophoric supramolecular materials. *Topics Curr. Chem.* **2023**, *381*, 2.
13 Luo, J.; Xie, Z.; Lam, J. W.; Cheng, L.; Chen, H.; Qiu, C.; Kwok, H. S.; Zhan, X.; Liu, Y.; Zhu, D.; Tang, B. Z. Aggregation-induced emission of 1-methyl-1,2,3,4,5-pentaphenylsilole. *Chem. Commun*. **2001**, 1740–1741.
14 Mei, J.; Leung, N. L.; Kwok, R. T.; Lam, J. W.; Tang, B. Z. Aggregation-induced emission: together we shine, united we soar! *Chem. Rev*. **2015**, *115*, 11718–11940.
15 Chen, J.; Law, C. C. W.; Lam, J. W. Y.; Dong, Y.; Lo, S. M. F.; Williams, I. D.; Zhu, D.; Tang, B. Z. Synthesis, light emission, nanoaggregation, and restricted intramolecular rotation of 1,1-substituted 2,3,4,5-tetraphenylsiloles. *Chem. Mater.* **2003**, *15*, 1535–1546.
16 Zhao, E.; Lam, J. W. Y.; Meng, L.; Hong, Y.; Deng, H.; Bai, G.; Huang, X.; Hao, J.; Tang, B. Z. Poly[(maleic anhydride)-*alt*-(vinyl acetate)]: a pure oxygenic nonconjugated macromolecule with strong light emission and solvatochromic effect. *Macromolecules* **2015**, *48*, 64–71.
17 Dou, X.; Zhou, Q.; Chen, X.; Tan, Y.; He, X.; Lu, P.; Sui, K.; Tang, B. Z.; Zhang, Y.; Yuan, W. Z. Clustering-triggered emission and persistent room temperature phosphorescence of sodium alginate. *Biomacromolecules* **2018**, *19*, 2014–2022.
18 Wang, Y.; Zhao, Z.; Yuan, W. Z. Intrinsic luminescence from nonaromatic biomolecules. *ChemPlusChem* **2020**, *85*, 1065–1080.
19 Xu, L.; Liang, X.; You, L.; Yang, Y.; Fen, G.; Gao, Y.; Cui, X. Temperature-sensitive poly(*N*-isopropylacrylamide)-chitosan hydrogel for fluorescence sensors in living cells and its antibacterial application. *Int. J. Biol. Macromol.* **2021**, *189*, 316–323.
20 Zhang, H.; Zhao, Z.; McGonigal, P. R.; Ye, R.; Liu, S.; Lam, J. W. Y.; Kwok, R. T. K.; Yuan, W. Z.; Xie, J.; Rogach, A. L.; Tang, B. Z. Clusterization-triggered emission: uncommon luminescence from common materials. *Mater. Today* **2020**, *32*, 275–292.
21 Yuan, W.; Zhang, Y. Nonconventional macromolecular luminogens with aggregation-induced emission characteristics. *J. Polym. Sci., Part A: Polym. Chem.* **2017**, *55*, 560–574.
22 Du, Y.; Xue, X.; Jiang, Q.; Huang, W.; Yang, H.; Jiang, L.; Jiang, B.;

Komarneni, S. Tunable multicolor luminescence polyglycidol-acrylates: one-pot preparation and properties. *ACS Appl. Polym. Mater.* **2023**, *5*, 3817–3826.
23 Cao, H.; Li, B.; Jiang, X.; Zhu, X.; Kong, X. Z. Fluorescent linear polyurea based on toluene diisocyanate: easy preparation, broad emission and potential applications. *Chem. Eng. J.* **2020**, *399*, 125867.
24 Jiang, X.; Wang, S.; Kong, X. Z. Quenching mechanism of PEG emission by pyrimidines and their detections using PEG as fluorescent sensor. *Chem. Eng. J.* **2023**, *468*, 143617.
25 Sun, C.; Jiang, X.; Li, B.; Li, S.; Kong, X. Z. Fluorescence behavior and mechanisms of poly(ethylene glycol) and their applications in Fe^{3+} and Cr^{6+} detections, data encryption, and cell imaging. *ACS Sustainable Chem. Eng.* **2021**, *9*, 5166–5178.
26 Wang, S.; Jiang, X.; Sun, C.; Kong, X. Z. Full green detection of antibiotic tetracyclines using fluorescent poly(ethylene glycol) as the sensor and the mechanism study. *ACS Biomater. Sci. Eng.* **2022**, *8*, 3957–3968.
27 Jiang, X.; Wang, Q.; Li, B.; Li, S.; Kong, X. Z. Fluorescence behavior and emission mechanisms of poly(ethylene succinamide) and its applications in Fe^{3+} detection and data encryption. *Chinese J. Polym. Sci.* **2023**, *41*, 129–142.
28 Wang, Q.; Li, B.; Cao, H.; Jiang, X.; Kong, X. Z. Aliphatic amide salt, a new type of luminogen: characterization, emission and biological applications. *Chem. Eng. J.* **2020**, *388*, 124182.
29 Li, S.; Pan, X.; Zhu, X.; Jiang, X.; Kong, X. Z. Uniform and fluorescent poly(urea-siloxane) microspheres: preparation and recyclable use as sensors for Cr^{6+} and Fe^{3+} detection. *ACS Appl. Polym. Mater.* **2023**, *5*, 3325–3337.
30 Li, L.; Li, S.; Cui, H.; Zhu, X.; Kong, X. Z. Phase transition and fluorescence emission of multiresponsive poly(ethylene glycol-*co*-siloxane) and its application for uric acid detection. *ACS Appl. Polym. Mater.* **2023**, *5*, 9413–9424.
31 Seuring, J.; Bayer, F. M.; Huber, K.; Agarwal, S. Upper critical solution temperature of poly(*N*-acryloyl glycinamide) in water: a concealed property. *Macromolecules* **2012**, *45*, 374–384.
32 Li, S.; Feng, S. High-sensitivity stimuli-responsive polysiloxane synthesized *via* catalyst-free aza-michael addition for ibuprofen loading and controlled release. *RSC Adv.* **2016**, *6*, 99414–99421.
33 Lian, L.; Wang, Q.; Duan, F.; Zhao, Y. Multi-tunable thermoresponsive behaviors of poly(amido thioether)s. *Polym. Chem.* **2024**, *15*, 83–96.
34 Zhou, C.; Chen, Y.; Huang, M.; Ling, Y.; Yang, L.; Zhao, G.; Chen, J. A new type of dual temperature sensitive triblock polymer (P(AM-*co*-AN)-*b*-PDMA-*b*-PNIPAM) and its self-assembly and gel behavior. *New J. Chem.* **2021**, *45*, 5925–5932.
35 Li, S.; Feng, L.; Lu, H.; Feng, S. From LCST to UCST: The phase separation behaviour of thermo-responsive polysiloxanes with the solubility parameters of solvents. *New J. Chem.* **2017**, *41*, 1997–2003.
36 Dong, X.; Cao, H.; Jiang, X.; Kong, X. Z.; Li, S. Phase transition and fluorescence emission characteristics of multi-responsive copolymer of oligo(ethylene glycol) methyl ether acrylate and methylacrylic acid. *Acta Polymerica Sinica* (in Chinese) **2019**, *50*, 1314–1321.
37 Sun, B.; Li, S.; Jiang, X.; Zhu, X.; Kong, X. Z. Synthesis of post-modified poly(ester-amino) microspheres *via* aza-Michael precipitation polymerization and its use for enzyme immobilization. *Polym. Adv. Technol.* **2021**, *32*, 1802–1812.
38 Pang, B.; Zhang, J.; Pang, M.; Zhao, P.; Yang, Z.; Feng, S.; Zhang, J. Design and preparation of a new polyurea-polysiloxane-polyether copolymer with a block soft segment prepared by utilizing aza-Michael addition reaction. *Polym. Chem.* **2018**, *9*, 869–877.
39 Li, S.; Yang, S.; Zhu, X.; Jiang, X.; Kong, X. Z. Easy preparation of superoleophobic membranes based on cellulose filter paper and their use for water-oil separation. *Cellulose* **2019**, *26*, 6813–6823.
40 Yıldız, M.; Demir, N.; Ünver, H.; Sahiner, N. Synthesis, characterization, and application of a novel water-soluble polyethyleneimine-based Schiff base colorimetric chemosensor for metal cations and biological activity. *Sensor Actuat. B* **2017**, *252*, 55–61.
41 Feng, K.; Li, S.; Feng, L.; Feng, S. Synthesis of thermo- and photo-responsive polysiloxanes with tunable phase separation *via* aza-Michael addition. *New J. Chem.* **2017**, *41*, 14498–14504.
42 Jung, H.; Jeon, S.; Jo, D. H.; Huh, J.; Kim, S. H. Effect of crosslinking on the CO_2 adsorption of polyethyleneimine- impregnated sorbents. *Chem. Eng. J.* **2017**, *307*, 836–844.
43 Jiang, X.; Zhu, X.; Arnold, A. A.; Kong, X. Z.; Claverie, J. P. Polyurea structure characterization by HR-MAS NMR spectroscopy. *Ind. Eng. Chem. Res.* **2017**, *56*, 2993–2998.
44 Lin, Y. S.; Lin, C. H.; Lee, W. F. Investigation of the synthesis and properties of the copolymeric hydrogels based on *N*-isopropyl acrylamide and acrylamidoazobenzene. *J. Polym. Res.* **2014**, *21*, 364.
45 Wu, P.; Siesler, H. W. The assignment of overtone and combination bands in the near infrared spectrum of polyamide 11. *J. Near Infrared Spectrosc.* **1999**, *7*, 65–76.
46 Li, Z.; Hao, B.; Tang, Y.; Li, H.; Lee, T. C.; Feng, A.; Zhang, L.; Thang, S. H. Effect of end-groups on sulfobetaine homopolymers with the tunable upper critical solution temperature (UCST). *Eur. Polym. J.* **2020**, *132*, 109704.
47 Fan, Y.; Zhang, J.; Shi, M.; Li, D.; Lu, C.; Cao, X.; Peng, C.; Mignani, S.; Majoral, J. P.; Shi, X. Poly(amidoamine) dendrimer-coordinated copper(II) complexes as a theranostic nanoplatform for the radiotherapy-enhanced magnetic resonance imaging and chemotherapy of tumors and tumor metastasis. *Nano Lett.* **2019**, *19*, 1216–1226.
48 Wang, G.; Fu, L.; Walker, A.; Chen, X.; Lovejoy, D. B.; Hao, M.; Lee, A.; Chung, R.; Rizos, H.; Irvine, M.; Zheng, M.; Liu, X.; Lu, Y.; Shi, B. Label-free fluorescent poly(amidoamine) dendrimer for traceable and controlled drug delivery. *Biomacromolecules* **2019**, *20*, 2148–2158.
49 Zhou, Q.; Liu, Y.; Wu, Y.; Li, Z.; Li, Y.; Liu, M.; Qu, T.; Chen, C. Measurement of mercury with highly selective fluorescent chemoprobe by carbon dots and silver nanoparticles. *Chemosphere* **2021**, *274*, 129959.
50 50 Wang, S.; Li, H.; Huang, H.; Cao, X.; Chen, X.; Cao, D. Porous organic polymers as a platform for sensing applications. *Chem. Soc. Rev.* **2022**, *51*, 2031–2080.
51 Ehsani, M.; Soleymani, J.; Mohammadalizadeh, P.; Hasanzadeh, M.; Jouyban, A.; Khoubnasabjafari, M.; Vaez-Gharamaleki, Y. Low potential detection of doxorubicin using a sensitive electrochemical sensor based on glassy carbon electrode modified with silver nanoparticles-supported poly(chitosan): a new platform in pharmaceutical analysis. *Microchem. J.* **2021**, *165*, 106101.
52 Ansar, S. M.; Jiang, W.; Mudalige, T. Direct quantification of unencapsulated doxorubicin in liposomal doxorubicin formulations using capillary electrophoresis. *Int. J. Pharmaceut.* **2018**, *549*, 109–114.
53 Yang, M.; Yan, Y.; Liu, E.; Hu, X.; Hao, H.; Fan, J. Polyethyleneimine-functionalized carbon dots as a fluorescent probe for doxorubicin hydrochloride by an inner filter effect. *Opt. Mater.* **2021**, *112*, 110743.
54 Singh, T. A.; Sharma, V.; Thakur, N.; Tejwan, N.; Sharma, A.; Das, J. Selective and sensitive electrochemical detection of doxorubicin via a novel magnesium oxide/carbon dot nanocomposite based sensor. *Inorg. Chem. Commun.* **2023**, *150*, 110527.
55 Mi, G.; Shi, H.; Yang, M.; Wang, C.; Hao, H.; Fan, J. Efficient detection doxorubicin hydrochloride using $CuInSe_2$@ZnS quantum dots and Ag nanoparticles. *Spectrochim. Acta A* **2020**, *241*, 118673.